Role of desmoplakin in supporting neuronal activity, neurogenic processes, and emotional-related behaviors in the dentate gyrus

Keisuke Otsubo[1,3], Naoko Sakashita[1,3], Yuki Nishimoto[1,3], Yo Sato[1], Takehisa Tsutsui[1], Katsunori Kobayashi[2], Kanzo Suzuki[1], Eri Segi-Nishida[1,*]

[1]Department of Biological Science and Technology, Faculty of Advanced Engineering, Tokyo University of Science, Tokyo, Japan

[2]Department of Pharmacology, Graduate School of Medicine, Nippon Medical School, Tokyo, Japan

[3] These authors equally contributed to this work

*Correspondence:

Eri Segi-Nishida,

6-3-1 Niijuku, Katsushika-ku, Tokyo, Japan, 125-8585

Email: eri.segi.nishida@rs.tus.ac.jp

Running title: Role of desmoplakin in DG

Keywords: desmoplakin, dentate gyrus, neurogenesis, anxiety, knockdown

Abstract

Desmoplakin (Dsp) is a component of desmosomal cell-cell junctions that interacts with the cadherin complex and cytoskeletal intermediate filaments. In addition to its function as an adhesion component, Dsp is involved in various biological processes, such as gene expression, differentiation, and migration. Dsp is specifically expressed in the hippocampal dentate gyrus (DG) in the central nervous system. However, it is unclear how Dsp impacts hippocampal function and its related behaviors. Using an adeno-associated virus knockdown system in mice, we provide evidence that Dsp in the DG maintains hippocampal functions, including neuronal activity and adult neurogenesis, and contributes to anxiolytic-like effects. Dsp protein is mostly localized in mature granule cells in the adult DG. Dsp knockdown in the DG resulted in a lowered expression of an activity-dependent transcription factor FosB, and an increased expression of mature neuronal markers, such as calbindin. In addition, the suppression of Dsp decreases serotonin responsiveness at the DG output mossy fiber synapses and alters adult neurogenic processes in the subgranular zone of the DG. Moreover, DG-specific Dsp knockdown mice showed an increase in anxiety-like behaviors. Taken together, this research uncovers an unexplored function for Dsp in the central nervous system and suggests that Dsp in the DG may function as a regulator to maintain proper neuronal activation and adult neurogenesis, and contribute to the adaptation of emotion-related behavior.

Introduction

Desmosomes are adhesive intercellular junctions that provide strong adhesion between cells and are abundant in tissues exposed to mechanical stress, such as the heart and skin. Mutations in these factors cause skin and heart vulnerability (Kowalczyk and Green, 2013). Desmosomal components comprise transmembrane cadherins, such as desmoglein and desmocollin, and intracellular proteins, such as plakoglobin, plakophilin, and desmoplakin (Dsp) (Garrod and Chidgrey, 2008; Broussard et al., 2015). Dsp is a family of plakin proteins that interacts with the cadherin/plakoglobin/plakophilin complex through the N-terminal domain and with an intermediate filament cytoskeleton through the C-terminal domain (Delva et al., 2009). In addition to mediating cell-to-cell adhesion, desmosomes function as cell signaling regulators involved in cell proliferation and differentiation (Johnson et al. 2014). In particular, Dsp is involved in processes such as gene expression, differentiation, and microtubule dynamics, indicating its diverse biological functions in addition to its function as an adhesion component (Bendrick et al., 2019; Dubash et al., 2016; Lombardi et al., 2016; Patel et al., 2014).

In the central nervous system, Dsp is specifically expressed in the hippocampal dentate gyrus (DG) in the brain (Yamasaki et al., 2008). The DG gates the flow of neocortical information into the hippocampal CA3 region and is one of the few areas of the mammalian brain where adult neurogenesis occurs (Drew et al., 2013; Zhao et al., 2008). It has been reported that Dsp is characterized as a molecular maker for neuronal maturation in the DG of hippocampus (Kobayashi et al., 2010). The expression level of *Dsp* in the DG increases with postnatal development, similarly to the patterns of other DG maturation markers, calbindin and tryptophan-2,3-dioxygenase 2 (Tdo2). Dsp transcription is directly regulated by Bcl11b, a transcription

factor that plays an important role in postnatal development of the DG (Simon et al., 2012). Forebrain neuron-specific knockout of Dsp in Emx1-Cre mice impairs progenitor proliferation and neuronal differentiation at 14 days postnatal age, indicating that Dsp contributes to the development of dentate granule neurons (Simon et al., 2012). However, whether Dsp regulates the function of dentate mature granule neurons and affects the process of adult neurogenesis in the DG remain unclear.

The hippocampus is a limbic structure implicated in the regulation of stress and pathophysiology/treatment of anxiety and depression (Segi-Nishida and Suzuki, 2022). We have previously demonstrated that long-term antidepressant treatment suppresses the expression of *Dsp* in the DG (Kobayashi et al., 2010; Imoto et al., 2017), indicating that Dsp plays a key role in emotion-related behaviors in the DG. Nevertheless, whether Dsp in the DG during adulthood is involved in emotion-related behaviors such as depression and anxiety is unclear.

In this study, we investigated the effect of Dsp knockdown in the DG on neuronal activation, adult hippocampal neurogenesis, and emotion-related behaviors using an adeno-associated virus (AAV) knockdown system in mice. We found that Dsp in the adult hippocampal DG maintains the function of dentate granule neurons, regulates neuronal differentiation during adult neurogenesis, and behaviorally contributes to anxiolytic-like effects.

Materials and Methods

Experimental animals

Seven-to-eight-week-old male C57BL/6N mice (23–25 g) were purchased from Japan SLC (RRID5295404; Hamamatsu, Japan). The mice were housed in groups of six per cage (32 cm length × 11 cm width × 13.5 cm height). All the mice were housed under standard conditions (temperature: 24 ± 2 °C, humidity: 55% ± 5%) with a 12 h light/dark cycle and *ad libitum* access to water and food (MR standard, Nosan Corporation, Yokohama, Japan). The weight gain of each mouse was recorded during the experiments to monitor their physical condition. All mice were habituated for longer than one week before the experimental procedures were performed. A total of 132 mice were used in this study (control animals, n=14; ECS-treated animals, n=6; fluoxetine-treated animals, n=7; AAV control miRNA infected animals, n=52; AAV Dsp miRNA infected animals, n=53). Animal use and procedures were conducted in according the Tokyo University of Science regulations on animal care and use in research and were approved by the Animal Care and Use Committee of Tokyo University of Science (approval numbers K20009, K21007, and K22007).

AAV preparation and hippocampal administration

AAVs (serotype rh10) expressing artificial microRNAs (miRNAs) targeting Dsp or control miRNAs with Emerald Green Fluorescent Protein (EmGFP) under the EF1α promoter were generated as follows: We designed the sequences for artificial microRNAs for Dsp according to the BLOCK-iT RNAi Designer website (Thermo Fisher Scientific). First, the DNA fragment encoding miRNA for *Dsp* (5'-TGC TGT TGA GAT GGA CAT CAA TGC ACG TTT TGG CCA CTG ACT GAC GTG CAT TGG TCC ATC TCA A-3' and 5'-CCT GTT GAG ATG GAC CAA TGC ACG TCA

GTC AGT GGC CAA AAC GTG CAT TGA TGT CCA TCT CAA C-3') was subcloned into pcDNA6.2-GW-EmGFP-miR using BLOCK-iT Pol II miR RNAi Expression Vector Kit (Invitrogen). The EmGFP and Dsp miRNA fragments were amplified by PCR from this vector and inserted between the KpnI and EcoRV sites of the pAAV-EF1α-DIO EYFP vector (#27056; Addgene). The resulting plasmid was named pAAV-EF1α-EmGFP-miR-Dsp. The DNA fragment encoding control microRNA (5′-TGC TGA AAT GTA CTG CGC GTG GAG ACG TTT TGG CCA CTG ACT GAC GTC TCC ACG CAG TAC ATT T-3′ and 5′-CCT GAA ATG TAC TGC GTG GAG ACG TCA GTC AGT GGC CAA AAC GTC TCC ACG CGC AGT ACA TTT C-3′), which can form a hairpin structure processed into mature microRNA but is predicted not to target any known vertebrate gene, was used to generate an AAV vector expressing control microRNA. TheBLOCK-iT Pol II miR RNAi Expression Vector Kit was used instead of those encoding Dsp miRNA. AAV particles were produced using the previously described procedure with minor modifications (Shinohara et al., 2018). Briefly, the AAVrh10 expression plasmid (Addgene #112866), pHelper vector (#240071, Agilent Technologies, Santa Clara, CA), and the constructed AAV-vector plasmid were transfected into AAV-293 cells (#240073, Agilent) using Lipofectamine 2000 (Thermo Fisher Scientific). Transfected AAV-293 cells were collected 72 h after transfection and resuspended in artificial cerebrospinal fluid. The cell suspensions were freeze-thawed three times. Cell debris was eliminated by centrifugation at 10,000 × g for 10 min and the supernatant containing the virus was collected. The viral suspension was incubated with benzonase (Merck Millipore, Burlington, MA, USA) to degrade residual DNA. The prepared AAV solution was aliquoted and stored at -80 °C. The AAV titer was quantified using PCR (5′-TGA GTC ACC CAC ACA AAG GA-3′ and 5′-CCA AGC TGG CCT AAC TTC AG-3′) after proteinase K treatment (Merck

137 Millipore). Under anesthesia with a mixture of medetomidine (0.3 mg/kg, ZENOAQ,
138 Japan), midazolam (4 mg/kg, Sandoz, Japan), and butorphanol (5 mg/kg, Meiji, Japan),
139 the mouse brain was fixed with stereotaxic instruments (Narishige, Tokyo, Japan). An
140 AAV solution of 500 nL per injection site (5.0×10^8 copies) was bilaterally injected
141 into the DG using a PV-820 Pneumatic PicoPump (World Precision Instruments,
142 Hessen, Germany) through a glass micropipette made with a PN-30 micropipette puller
143 (Narishige). The stereotaxic coordinates were targeted to the ventral DG: 3.2 mm
144 posterior to the bregma, 2.7 mm lateral to the midline, and 3.0 mm ventral to the skull
145 surface at the bregma, according to the mouse brain atlas (Paxinos and Franklin, 2012).
146 Data were excluded from the analysis if fluorescence was not observed in the DG.
147

148 **Electroconvulsive stimulation and drug treatment**

149 Bilateral ECS (current, 25–35 mA; shock duration, 1 sec; frequency, 100 pulse/sec;
150 pulse width, 0.5 msec) was administered with a pulse generator (ECT Unit; Ugo Basile,
151 VA, Italy) to mice as described previously (Imoto et al., 2017). ECS was administered
152 4 times a week. Fluoxetine hydrochloride (LKT Labs, St. Paul, MN, USA) was
153 dissolved in drinking water and orally applied at a dose of 22 mg/kg/day for 4 weeks
154 as described previously (Kobayashi et al., 2010).
155

156 **RNA extraction and real-time PCR**

157 Seven to eight weeks after AAV infection, the mice were decapitated under deep
158 anesthesia, coronal brain slices (1 mm) were cut using a tissue slicer, and the DG of the
159 hippocampus was dissected. Total RNA was extracted using the Reliaprep RNA Cell
160 Miniprep System (Promega, Madison, WI, USA) and reverse transcribed using
161 ReverTra Ace (Toyobo, Osaka, Japan). Subsequent, real-time PCR was performed

162 using the StepOne system (Applied Biosystems, Foster City, CA) and Thunderbird
163 SYBR qPCR mix (Toyobo). The expression levels of each gene were quantified using
164 standardized external dilutions. The relative expression levels of the target genes were
165 normalized to those of 18S rRNA or *Gapdh*. The specificity of each primer set was
166 confirmed by melt-curve analysis, and the product size was examined using gel
167 electrophoresis. Table 1 summarizes the primer sequences for each gene.
168
169 **Electrophysiological analysis**
170 Mice were decapitated under deep anesthesia 7–8 weeks after AAV infection, and both
171 hippocampi were isolated. Transverse hippocampal slices (380 μm) were cut in ice-cold
172 saline using a tissue slicer (7000smz, Campden Instruments Ltd., Leics, UK). The slices
173 were then incubated for 30 min at 30 °C and maintained in a humidified interface-
174 holding chamber at room temperature before use. Intense GFP fluorescence in the DG
175 and the mossy fiber (MF) tract was confirmed, and electrophysiological recordings
176 were performed as described (Kobayashi et al., 2010, 2020). Electrophysiological
177 recordings were made in a submersion-type chamber maintained at 27.0–27.5 °C and
178 superfused at 2 mL/min with recording saline composed of (in mM): NaCl, 125; KCl,
179 2.5; NaH2PO4, 1.0; NaHCO3, 26.2; glucose, 11; CaCl2, 2.5; MgCl2, 1.3 (equilibrated
180 with 95% O2 / 5% CO2). For recording field excitatory postsynaptic potentials (EPSPs)
181 arising from the medial perforant path (MPP)-granule cell synapse, a glass recording
182 pipette filled with 2 M NaCl and bipolar tungsten stimulating electrodes were placed in
183 the middle third of the molecular layer in the dentate gyrus. The input output
184 relationship at the MPP input was examined by changing the stimulating intensity from
185 1.5 to 6 V. The initial slope of the EPSPs was measured. Field EPSPs arising from the
186 MF synapses were evoked by stimulating the dentate granule cell layer and were

recorded from the stratum lucidum of CA3. The amplitude of field EPSPs was measured with a 0.5-ms window positioned at 70–80% of the peak of the baseline field EPSPs. More than 85% block of EPSP by an agonist of group II metabotropic glutamate receptors (2*S*,2'*R*,3'*R*)-2-(2',3'-dicarboxycyclopropyl) glycine (DCG-IV, 1 μM) was the criterion used to identify MF input. A single electrical stimulation was delivered at a frequency of 0.05 Hz. All recordings were performed using a Multiclamp 700 B amplifier (Molecular Devices, Sunnyvale, CA, USA), filtered at 2 kHz, and stored on a personal computer via an interface (digitized at 10 kHz). Data were obtained from distinct samples. Serotonin hydrochloride was purchased from Sigma-Aldrich.

Sample isolation for immunohistochemistry

Five'-bromo-2'-deoxyuridine (BrdU, 150 mg/kg, Nacalai Tesque, Japan) was intraperitoneally administered to mice once 2 h before sacrifice to evaluate cell proliferation to label the dividing cells, or four times on 14 and 15 days (twice a day) before sacrifice to evaluate cell survival.

For Dsp immunostaining, the mice were deeply anesthetized and transcardially perfused with cold saline. The brains were then stored at -80°C until further use. Serial fresh frozen sections (18 μm thick) were cut through the entire hippocampus using a cryostat (Leica 1510, Leica Microsystems, Wetzlar, Germany) and stored at -80°C. For other immunostaining procedures, mice were deeply anesthetized and perfused with cold saline followed by 4% paraformaldehyde (Sigma-Aldrich) in 0.1 M phosphate buffer (pH 7.4) and were post-fixed at 4 °C for 48 h. The brains were then cryoprotected in 20% sucrose for 48 h and in 30% sucrose for 24 h and stored at -80°C until further use. Serial sections (30 μm thick) were cut through the entire hippocampus using a

211 cryostat and stored in 30% glycerol and 30% ethylene glycol in 0.02 M phosphate
212 buffer (pH 7.4) at -20 °C until staining.
213
214 **Immunohistochemistry**
215 For Dsp/NeuN or Dsp/NeuroD1 immunostaining, fresh frozen sections were fixed with
216 100% methanol for 20 min at 4 °C. After fixation, the sections were washed with
217 phosphate-buffered saline (PBS), blocked using 10% equine serum in PBS, and
218 incubated with monoclonal mouse anti-Dsp (1:50; Progen, 61003, RRID:AB_2920666)
219 and rabbit anti-NeuN (1:500, Abcam, ab177487, RRID:AB_2532109) or rabbit anti-
220 NeuroD1 (1:500; Abcam, ab213725, RRID:AB_2801303) at 4 °C overnight. After
221 washing with PBS, the sections were incubated with donkey anti-mouse IgG antibody
222 conjugated to Alexa Fluor 488 (1:300; Thermo Fisher Scientific, RRID:AB_141607)
223 and donkey anti-rabbit IgG antibody conjugated to Alexa Fluor 555 (1:1000; Thermo
224 Fisher Scientific, RRID:AB_162543) for 60 min. The sections were then incubated with
225 4',6-diamidino-2-phenylindole (DAPI; 1:5,000; Merck Millipore) and covered with
226 Mowiol (Merck Millipore) after washing with PBS. Confocal images were taken using
227 Olympus FV3000. Single confocal images were shown for localization of Dsp. Anti-
228 Dsp and rabbit anti-mouse IgG antibody conjugated to Alexa 555 (1:300; Thermo
229 Fisher Scientific, RRID:AB_2535848) were used to confirm Dsp knockdown.
230 For FosB, NeuroD1, SOX2, and doublecortin (DCX) immunostaining, the 30
231 μm thick floating sections were washed with PBS and blocked using 10% equine serum
232 (SH30074; Cytiva) in PBS containing 0.3% Triton X-100 (PBST) at room temperature
233 for 60 min, followed by overnight incubation with rabbit anti-FosB (1:1000; Abcam,
234 ab184938, RRID: AB_2721123), goat anti-SOX2 (1:200; Santa Cruz, sc17320,
235 RRID:AB_2286684), rabbit anti-NeuroD1 (1:1000), rabbit anti-doublecortin (DCX)

236 (1:1000; Cell Signaling Technology, Danvers, MA, USA; RRID:AB_561007) at 4 °C.
237 For BrdU or BrdU/NeuN immunostaining, the floating sections were incubated in 50%
238 formamide in 2×saline sodium citrate buffer (SSC) for 2 h at 60 °C, followed by
239 incubation in 2 M hydrogen chloride at 37 °C for 30 min, and neutralized with 0.1 M
240 boric acid (pH 8.5) at room temperature for 10 min before blocking. After blocking, the
241 sections were incubated overnight with monoclonal rat anti-BrdU (1:8000; Abcam,
242 ab6326, RRID:AB_305426) and rabbit anti-NeuN (1:500) at 4°C. After washing with
243 PBST, the sections were incubated with donkey anti-rabbit IgG antibody conjugated to
244 Alexa Fluor 555 (1:1000 for NeuroD1 and FosB immunostaining; Thermo Fisher
245 Scientific, RRID:AB_2535853) or conjugated to Alexa Fluor 647 (1:1000 for NeuN
246 immunostaining; Thermo Fisher Scientific, RRID: RRID:AB_162542), donkey anti-
247 goat IgG antibody conjugated to Alexa Fluor 555 (1:1000 for SOX2 immunostaining;
248 Thermo Fisher Scientific, RRID:AB_141788) and donkey anti-rat IgG antibody
249 conjugated to Alexa Fluor 555 (1:1000 for BrdU immunostaining; Abcam, RRID:
250 AB_2813834) for 60 min. After washing with PBST, the sections were incubated with
251 DAPI (1:10,000) and mounted on slides with Mowiol after washing with PBS. For DCX
252 immunostaining, the sections were incubated with biotinylated goat anti-rabbit IgG
253 (1:200; Vector Laboratories Inc., Burlingame, CA, USA; BA1000, RRID:
254 AB_2313606) for 60 min. The sections were washed with PBST and incubated with the
255 ABC Vectastain Kit (Vector), and antigen detection was performed with 0.06% 3,3'-
256 diaminobenzidine (Wako) staining. After washing, the sections were mounted on slides
257 using Entellan New (Merck Millipore). Sections were photographed under a
258 microscope (BZX-700, Keyence, Osaka, Japan).
259
260 **Quantification of BrdU-, SOX2-, NeuroD1-, DCX-, and FosB-positive cells**

Computer-assisted image analysis (ImageJ, NIH, Bethesda, MD, USA; QuPath, Bankhead et al., 2017) was used for cell analysis. For quantification of FosB-positive cells, three hippocampal sections with EGFP-expressing DG were photographed. The number of FosB-positive cells was counted and presented as the number of cells per 10,000 μm^2 area in the granule cell layer of the DG. For BrdU-labeled cell quantification, 6–8 hippocampal sections with EGFP-expressing DG were photographed. To evaluate cell proliferation, the number of BrdU-positive cells was counted in the subgranular zone (SGZ) and presented as the number of cells per 1,000 μm along the SGZ. To evaluate cell survival, the number of BrdU-positive cells in the granule cell layer of the DG was counted and presented as the number of cells per 100,000 μm^2 of the granule cell layer. To evaluate NeuN colocalization of BrdU (+) cells, z-sectioning was used to determine if BrdU (+) cells were colabeled with NeuN. At least 30 BrdU (+) cells per animals were analyzed for co-localization with NeuN. For SOX2- or NeuroD-positive cell quantification, 3–4 hippocampal sections with EGFP-expressing DG were photographed. The number of SOX2- or NeuroD1-positive cells in the SGZ was counted and presented as the number of cells per 1,000 μm along the SGZ. For DCX-positive cell quantification, 2–3 hippocampal sections with EGFP-expressing DG were photographed. DCX-positive cells in which dendrites reached the molecular layer and underwent complex processes were subcategorized as DCX-positive cells with long and branched dendrites. The total number of DCX-positive and DCX-positive cells with long dendrites was counted in the SGZ and presented as the number of cells per 100 μm along the SGZ.

Golgi staining

285 Golgi staining was performed using a FD Rapid Golgi Stain Kit (PK401, FD Neuro
286 Technologies) according to the manufacturer's instructions. Briefly, mice were
287 sacrificed by decapitation at 24 h after the social interaction test, and the brains were
288 quickly collected in MilliQ water. The hippocampal part of the brain was dissected and
289 immersed in freshly prepared Golgi-Cox impregnation buffer included in the kit. The
290 impregnation buffer was refreshed after 24 h, and the brains were incubated for 2 weeks.
291 After cryoprotection with the cryoprotectant buffer included in the kit at 4°C for 1 week,
292 each brain was frozen and kept at 80°C and cut into 100-μm sections with a cryostat.
293 The sections were mounted on gelatin-coated slides, dried for 72 h, and stained
294 according to the manufacturer's instructions. The slides were dehydrated in ethanol,
295 cleared in xylene, and covered with Entellan New. The sections were photographed
296 under a microscope (BZX-700, Keyence, Osaka, Japan). The total number of spines in
297 dendrites of Golgi-impregnated granule neurons in the inner molecular layer in the DG
298 were counted. ImageJ was used to measure dendritic length. Analysis was performed
299 on 10 dendrites in per mouse (n=6 each group).
300
301 **Behavioral experiments**
302 The mice were habituated to the testing room for at least 30 min before the behavioral
303 test. During the test, the movement of each mouse was recorded using a digital video
304 camera. All records were stored and analyzed using the SMART 3.0 video tracking
305 software (Panlab, Barcelona, Spain, RRID: SCR_002852). The apparatus was
306 thoroughly cleaned with 70% ethanol after the removal of each mouse.
307 The open field test (OFT) was performed for 10 min using an apparatus
308 composed of opaque white walls and a floor (50 cm × 50 cm × 20 cm) illuminated at
309 an intensity of 80 lux in the center of the floor. Each mouse was placed in the center of

310 an open-field arena, and locomotor activity was recorded for 10 min. The total distance
311 moved, relative time spent in the central zone, and entry time into the central zone were
312 measured. The floor was divided into 25 squares, and the four central squares were
313 defined as the central zone.

314 The forced swim test (FST) was performed in a cylindrical container (13 cm
315 diameter, 25.5 cm height) filled with water to a height of 18 cm. Water (23–25 °C) was
316 replaced between the trials. The FST was performed and recorded for 10 min using a
317 digital video camera. The duration of immobility was then quantified.

318 The spontaneous locomotor activity (LMA) test was performed in a transparent
319 home cage without bedding (20 cm length × 12.5 cm width) over 60 min. The total
320 distance moved during the last 30 min was tracked.

321 The compartment social interaction test (SIT) was performed in an SIT
322 apparatus (LE894T, Panlab) consisting of three chambers (42 cm × 60 cm × 22 cm) and
323 two partitions (5.5 cm × 0.15 cm × 17 cm). Each mouse was placed in the middle
324 chamber and allowed to explore the chamber freely for 5 min. Immediately after
325 habituation, an unfamiliar mouse (a 7–8-week-old male C57BL/6N mouse) was
326 introduced into one of the two side chambers enclosed in a wire cage. An identical
327 empty wire cage was placed on the opposite side of the chamber. After placement, the
328 side doors were opened simultaneously, and the test mouse was allowed to explore the
329 entire three-chamber arena for 10 min. The time spent in each compartment was
330 measured.

331 An elevated plus maze (EPM) test was performed in an EPM apparatus (EPM-
332 X, Muromachi Kikai, Japan) consisting of two open arms (30 cm × 6 cm, 40 lux) and
333 two closed arms (30 cm × 6 cm × 15 cm, 20 lux) extending from a central platform (6
334 cm × 6 cm). The maze was elevated to 40 cm above the floor. Each mouse was placed

in the center of the maze, facing the open arm, and allowed to explore freely for 10 min. The total distance and time spent in the open arms were measured.

Statistical analyses

All data are presented as the mean ± standard error of the mean. Statistical analyses were performed using an unpaired Student's *t*-test, Welch's *t*-test or two-way analysis of variance (ANOVA). Statistical significance was set at $P < 0.05$. Before performing *t*-test, normality of the data was examined using the Shapiro–Wilk test. Detailed statistical data are presented in Table 2. Outliers in data from Fig. 5B were removed using the Grubb's outlier test. Otherwise, we did not exclude samples from statistical analysis. All analyses were performed using the PRISM 9 software (GraphPad, San Diego, CA, USA).

347 ## Results

348 **Expression of Dsp in the hippocampal DG and its regulation by antidepressant**
349 **stimulation**

350 *Dsp,* a granule cell-specific maturation marker (Yamasaki et al., 2008; Kobayashi et al.,
351 2010), is highly and specifically expressed in the DG of the hippocampus of the central
352 nervous system (Fig. 1A, Allen Institute for Brain Science, 2004). However, the
353 localization of Dsp protein in the DG has not been fully investigated. Therefore, we
354 initially examined the cellular localization and cell type of Dsp expression.
355 Immunohistological analysis revealed that Dsp was highly expressed in the granule cell
356 layer and molecular layer in the DG compared to the CA1 region (Fig. 1B). Dsp
357 immunoreactivity signals were detected in NeuN-positive cells in the DG (Fig. 1C,
358 upper). However, Dsp signals were rarely detected in NeuroD1-positive neural
359 progenitors or immature neurons in the SGZ of the DG (Fig. 1C, lower, arrows). These
360 findings suggest that Dsp is expressed in mature granule neurons in the DG. Dsp
361 immunostaining was only observed after methanol fixation; therefore, the localization
362 of other neuronal markers such as an immature neuronal marker DCX was not
363 investigated.

364 Furthermore, we investigated whether Dsp expression was regulated by
365 antidepressant stimulation at the protein level. The expression of *Dsp* in the DG was
366 reduced by chronic administration of electroconvulsive seizure (ECS) or a selective
367 serotonin reuptake inhibitor (SSRI) (Fig. 1D), as previously reported (Imoto et al.,
368 2017). Immunostaining analysis showed that Dsp protein began to decrease in outer
369 and inner granule neurons at 11 times of ECS, and its expression almost disappeared at
370 20 times of ECS administration (Fig. 1E). Thus, suppression of desmoplakin protein

371 expression by antidepressant treatments would be expected to require a longer time or
372 stimulus than suppression of mRNA expression.
373
374 **Dsp expression knockdown in the DG by an adeno-associated virus (AAV)**
375 **carrying Dsp miRNA**
376 To explore the role of Dsp in hippocampal function, we performed an AAV-mediated
377 knockdown of Dsp in the DG. For this purpose, we generated AAVrh10 expressing
378 EGFP and an artificial miRNA targeting Dsp mRNA (AAV-Dsp miRNA; Fig. 2A). The
379 AAV rh10 serotype shows high transduction efficiency into granule neurons in the DG
380 (Sehara et al., 2022). Seven to eight weeks after the injection of AAV-Dsp or AAV-
381 control miRNA into the DG, strong EGFP signals, which were co-expressed with
382 miRNA, were observed in the molecular layer and granule cell layer in the DG and
383 CA3 projection area (Fig. 2A, left). EGFP signals did not co-localize in DCX-positive
384 cells in the DG (Fig. 2A, right), indicating that AAV-mediated gene transfer occurs
385 primarily in mature granule neurons of the DG. *Dsp* mRNA expression significantly
386 decreased in the AAV-Dsp miRNA group (Fig. 2B). Moreover, immunohistological
387 analysis showed a decrease in Dsp immunoreactivity in the DG following AAV-Dsp
388 miRNA injection (Fig. 2C), demonstrating that the sequence of artificial miRNAs
389 targeting Dsp used in this study has the potential to knockdown Dsp expression.
390
391 **Changes in activity marker expression and spine number in the DG and alteration**
392 **of the sensitivity to serotonin at the MF synapse by Dsp knockdown**
393 First, we examined the direct effect of Dsp knockdown on the activity of dentate granule
394 neurons. FosB, including ΔFosB, is induced in response to many types of chronic
395 stimuli and accumulates because of its high stability (Nestler et al., 1999; Lamothe-

396 Molina et al., 2022). Consequently, we performed immunohistochemical analysis using
397 an anti-FosB antibody to monitor neuronal activity in the DG under normal home-cage
398 conditions. FosB immunoreactivity in the granule cell layer of the DG significantly
399 decreased in the Dsp knockdown group (Fig. 2D).

400 Because Dsp is a granule cell-specific DG maturation marker (Yamasaki et al.,
401 2008; Kobayashi et al., 2010), we examined the expression of other markers, including
402 *Calb, Tdo2, Ntf3, and Il1r1* in the DG. The expression of *Calb, Tdo2,* and *Ntf3*
403 significantly increased in the DG of the Dsp knockdown group (Fig. 2E).

404 Electrophysiological analyses of synaptic transmission were further performed
405 using acute hippocampal slices (Fig. 3A-I). We first examined the input-output
406 relationship of MPP-granule cell synaptic transmission by changing the intensity of
407 stimulation (Fig. 3A). No significant change in the relationship between fiber volley
408 amplitude and EPSP slope was observed (Fig. 3B and C). Next, properties of DG output
409 MF-CA3 synaptic transmission were examined (Fig. 3D) and there was no change in
410 the ratio of field EPSP to fiber volleys (Fig. 3E). These results suggest that the basal
411 transmission efficacy at the MPP-granule cell and the MF-CA3 synapses was not
412 altered by Dsp knockdown. Antidepressant treatment attenuates the synaptic facilitation
413 induced by repetitive stimulation and augments serotonergic modulation at the MF
414 synapse (Kobayashi et al., 2010; Imoto et al., 2017; Kobayashi et al., 2020). Dsp
415 knockdown did not change synaptic facilitation after 1 Hz stimulation (Fig. 3F and G).
416 Bath-applied serotonin induced the potentiation of field EPSPs in the AAV control
417 group (Fig. 3H), consistent with the findings of previous studies. The magnitude of
418 serotonin-induced potentiation was significantly reduced in the Dsp knockdown group
419 (Fig. 3H and I). To further investigate the role of Dsp in spine formation in the granule
420 neurons, we employed Golgi staining to assess spine number of granule cell dendrites

421 in the inner molecular layer (Fig. 3J). Dsp knockdown slightly but significantly
422 decreased the total number of spines (Fig. 3K).
423
424 **Changes in neurogenic activity in the DG by Dsp knockdown**
425 Adult hippocampal neurogenesis consists of proliferation, differentiation, and survival
426 and is regulated by various factors, including signals from adjacent mature granule
427 neurons in the DG (Kempermann et al., 2015). Since the above results suggest that Dsp
428 regulates neuronal activation in the DG, we explored the influence of Dsp knockdown
429 on hippocampal neurogenesis. First, we examined the effect of Dsp knockdown on cell
430 proliferation. BrdU was administered 2 h before the sacrifice to label proliferating cells
431 (Fig. 4A, left). BrdU-positive cells were detected in the SGZ of the DG (Fig. 4A,
432 middle), and no difference was observed in the number of proliferating cells between
433 the control and Dsp knockdown groups (Fig. 4A, right). We next examined the number
434 of SOX2-positve cells in the SGZ. SOX2 is a marker for neural stem cells and
435 progenitors in the adult DG (Segi-Nishida et al., 2008). There was no difference in the
436 number of SOX2-positive cells in the SGZ (Fig. 4B). We then examined the expression
437 of Neuro D1, which is expressed in progenitors/neuroblasts and immature neurons in
438 the adult DG. The number of NeuroD1-positive cells in the SGZ was significantly
439 decreased in the Dsp knockdown group (Fig. 4C). We further examined the expression
440 of the immature neuronal marker, DCX, in the DG. The total number of DCX-positive
441 cells and those with long dendrites decreased in the Dsp knockdown group (Fig. 4D).
442 Because most newborn cells in the DG die within 2–3 weeks following proliferation in
443 mice (Ueno et al., 2019), we evaluated the effect of Dsp knockdown on the survival of
444 newborn cells 2 weeks after BrdU administration (Fig. 4E, left). The number of BrdU-
445 positive cells in the DG showed a tendency to decrease, yet there was no significant

446 difference between the control group and the Dsp knockdown group (Fig. 4E, middle).
447 Furthermore, there was no difference in the ratio of NeuN-positive cells among the
448 BrdU-positive cells.
449
450 **Influence of Dsp knockdown on anxiety-related behaviors**
451 The ventral DG is a key brain region involved in emotional behaviors, including
452 anxiety- and depression-like behaviors (Sahay and Hen, 2007; Levone et al. 2015;
453 Anacker et al. 2018). To examine the influence of Dsp knockdown in the DG on
454 emotion-related behaviors, we conducted three sets of behavioral experiments (Fig. 5A).
455 First, we performed an open-field test to assess behavior in an anxiety-provoking
456 environment. Dsp knockdown in the DG suppressed locomotor activity and the number
457 of entries into the central area in the open field box, and a suppressive trend was
458 observed for the time spent in the central area (Fig. 5B). Next, we evaluated immobility
459 time in the FST to assess depression-like behavior. No difference in immobility time
460 between the control and Dsp knockdown groups was observed (Fig. 5C). Another set
461 of experiments was conducted on locomotor activity in a home cage, social interaction
462 test, and elevated plus maze test. Contrary to the data from the open field test, both
463 control and knockdown groups demonstrated comparable locomotor activity under
464 standard conditions (Fig. 5D), suggesting that the knockdown does not perturb baseline
465 locomotor function. In the three-chamber social interaction test, the control mice spent
466 more time around the area with an unfamiliar mouse than around the area with empty
467 cages. This social interaction behavior was comparable to that observed in the Dsp
468 knockdown mice (Fig. 5E). In the elevated plus maze test, a reduction in both the time
469 spent in the open arm and locomotor activity was observed in Dsp knockdown mice
470 (Fig. 5F). These results demonstrate that Dsp knockdown mice in the DG shows

anxiety-like behavior. Also, these findings can implicate that expression of Dsp in the DG plays an anti-anxiety role.

Discussion

This study aimed to investigate the role of Dsp expressed in the DG in hippocampal function and emotion-related behaviors. We showed that Dsp is localized mostly in mature granule neurons in the DG and that knockdown of Dsp decreases the expression of neuronal activity marker and serotonin responsiveness in DG neurons while enhancing the expression of mature neuronal markers. In addition, we demonstrated that Dsp knockdown in the DG alters adult neurogenic processes in the adjacent SGZ and that these hippocampal changes contribute to anxiety-like behaviors. These findings suggest that Dsp in the DG maintains the activity of mature neurons, regulates neuronal differentiation in the adult neurogenic process, and contributes to anxiolytic-like effects. This study is the first to demonstrate the role of Dsp in neuronal activity and emotion-related behaviors in the DG.

Expression of desmoplakin in the DG

Since Dsp could play an important role in cell-to-cell adhesion and subsequent intracellular regulatory signaling, we initially confirmed its localization in the brain. Immunohistological studies showed that Dsp protein was localized in granule cell layer in the DG (Fig. 1B). Dsp colocalized with the NeuN-positive cells, but not with the neural progenitor/immature neuron marker NeuroD1-positive cells in the DG (Fig. 1C). These results are consistent with those of a previous study that demonstrated that Dsp colocalizes with the post-mitotic neuron marker Bcl11b but not with the neural stem cell/progenitor marker SOX2 in the DG at 14 days of postnatal age (Simon et al., 2012).

Desmosome components include transmembrane cadherins and intracellular proteins such as plakoglobin, plakophilin, and Dsp (Garrod and Chidgrey, 2008; Broussard et al., 2015). Nevertheless, electron microscopy images of the rat DG showed

498 no desmosome structures between the cell bodies (Laatsch and Cowan, 1966).
499 Therefore, Dsp in the DG may form a complex different from that in epithelial
500 desmosomes. The expression and interactions of each desmosome component in the
501 DG will be examined to elucidate the localization and function of Dsp in neurons.
502
503 **Role of desmoplakin in mature granule neurons in the DG**
504 We found that Dsp knockdown in the DG suppressed FosB expression (Fig. 2D); FosB
505 is useful for monitoring steady-state activation. FosB, including ΔFosB, is induced in
506 response to many types of stimuli and shows high stability (Nestler et al., 1999;
507 Lamothe-Molina et al., 2022). In contrast, Dsp knockdown increased the expression of
508 the mature neuronal markers *Calb1*, *Tdo2*, and *Ntf3* (Fig. 2E), which are negatively
509 regulated by strong neuronal activation, such as in the ECS and epileptic seizures
510 (Imoto et al., 2017; You et al., 2017). Although the number of dendritic spines in DG
511 neurons was slightly but significantly reduced by Dsp knockdown, electrophysiological
512 analysis showed that Dsp suppression did not alter the basal transmission efficiency at
513 the MPP-granule cells. Excitatory inputs other than the MPP input may be altered,
514 resulting in attenuated granule cell activity. It is also possible that Dsp knockdown
515 affected inhibitory synapses or intrinsic excitability of granule cells.
516 Dsp suppression did not alter the basal transmission efficiency at the MF-CA3
517 synapses; however, it reduced serotonin-induced potentiation (Fig. 3). Synaptic
518 potentiation by serotonin is mediated by presynaptic 5-HT4 receptor-cAMP signaling
519 in the MF, which is enhanced by antidepressant treatment including ECS (Kobayashi et
520 al., 2008; 2020). Dsp knockdown in the DG may reduce serotonin-mediated
521 intracellular signaling in the DG.

522 Dsp is involved in various biological processes such as gene expression,
523 differentiation, and cell migration (Bendrick et al., 2019; Dubash et al., 2016; Lombardi
524 et al., 2016; Patel et al., 2014). Dsp interacts with plakoglobin, also known as γ-catenin
525 (Delva et al., 2009). Suppression of Dsp expression in atrial myocyte cell lines leads to
526 nuclear localization of plakoglobin/γ-catenin (Garcia-Gras et al., 2006). Further detail
527 analysis will be required to characterize the Dsp-mediated transcriptional pathway.
528 Especially, confirmation of the nuclear translocation of plakoglobin/γ-catenin will
529 clarify whether changes in the expression of these factors are mediated by catenin
530 signaling.
531
532 **Influence of desmoplakin knockdown on the neurogenic process in the DG**
533 Adult neurogenesis in the SGZ of the DG is regulated by various signals from
534 surrounding neurons (Kempermann et al., 2015). We investigated the role of Dsp in
535 several neurogenic processes in the DG. Suppression of Dsp reduced the number of
536 NeuroD1-positive neural progenitors and DCX-positive immature neurons, whereas the
537 number of proliferating cells and SOX2-positive neural stem/progenitor cells remained
538 unchanged (Fig. 4). EGFP signals, which should be coexpressed with miRNA, were not
539 observed in DCX-positive cells of the DG (Fig. 2A), suggesting that Dsp in the DG
540 indirectly regulates neurogenic processes in the adjacent SGZ. Since the rate of NeuN-
541 positive neuronal differentiation at 14 days of cell age did not change between the
542 control and Dsp knockdown, the period of NeuroD1 and DCX expression may be
543 shortened. Thus, it is possible that Dsp knockdown promoted the rate of differentiation
544 of newborn neurons, which allowed them to progress to maturity without sufficient
545 differentiation. Forebrain neuron-specific ablation of Dsp impairs developmental
546 hippocampal neurogenesis (Simon et al., 2012). During postnatal development in this

547 mutant line, cell proliferation and neural differentiation in the DG were suppressed. All
548 these findings suggest that Dsp is important for the regulation of cell proliferation
549 during developmental neurogenesis and for neural differentiation during both
550 developmental and adult neurogenesis.

551 How does Dsp indirectly regulate neuronal differentiation in post-mitotic
552 neurons? Neuronal activation, such as that in the ECS, promotes the expression of adult
553 neurogenic factors such as *Vegf*, *Fgf2*, and *Wnt2* in the DG (Newton et al., 2003;
554 Warner-Schmidt et al., 2007). Conversely, the suppression of neuronal activity in the
555 DG by inhibiting Dsp expression may reduce the expression of these growth factors.
556 Furthermore, intracellular skeletal regulation by Dsp may also affect neurogenic niche
557 formation. The neurogenic niche provides a unique milieu containing an extracellular
558 matrix, humoral factors, and cell-cell contacts that allow controlled neuronal
559 development (Kempermann et al., 2015). Altering the cytoskeleton of dentate granule
560 neurons may affect intercellular contacts and extracellular matrix adhesion and inhibit
561 neurogenic niche formation.

562

563 **Desmoplakin in the DG as a key regulator for emotion-related behaviors**

564 The DG of the hippocampus controls emotion-related behaviors (Segi-Nishida and
565 Suzuki, 2022). Although Dsp knockdown in the DG did not affect baseline locomotor
566 function, depression-like behavior, or social behavior, it reduced the time spent in the
567 open arm in the EPM test and reduced activity in the novel open field and EPM
568 environments designed to elicit anxiety (Fig. 5), indicating an environment-specific
569 anxious-like alteration following Dsp knockdown. The hippocampus plays functionally
570 distinct roles in the dorsal and ventral regions (Fanselow and Dong, 2010). The dorsal
571 region is involved in stress-induced learning and memory changes, and the ventral

572 region contributes to stress responses and emotions such as anxiety. Because AAV was
573 injected into the ventral DG area in this study (as described in the Methods section),
574 Dsp in the ventral DG may play an anxiolytic-like role.

575 In animal models, chronic antidepressant treatment induces anxiolytic-like
576 effects (Santarelli et al., 2003) and promotes the differentiation of newborn neurons in
577 the DG (Wang et al., 2008; Ueno et al., 2019), while suppressing the expression of
578 mature markers, including *Dsp,* in the DG (Fig. 1; Kobayashi et al., 2010; Imoto et al.,
579 2017). The loss of Dsp function in the DG may lead to anxiolytic effects; however,
580 surprisingly, anxiety-like behavior was observed (Fig. 5). Previous findings indicated
581 that adult neurogenesis in the DG affects anxiety-like behaviors. For instance,
582 transgenic mice in which adult neurogenesis was suppressed by the expression of the
583 pro-apoptotic protein BAX in neural progenitor cells show increased anxiety-related
584 behaviors (Revest et al., 2009). Therefore, suppression of adult neurogenesis in the DG
585 by Dsp knockdown may promote anxiety-like behaviors.

586 Furthermore, acute activation of the ventral DG by channelrhodopsin in
587 proopiomelanocortin (POMC)-Cre mice suppresses anxiety-like behavior in the EPM
588 (Kheirbek et al., 2013). Because our findings showed that Dsp knockdown in the DG
589 reduced the expression of the neuronal activity marker FosB (Fig. 2D), the suppression
590 of neuronal activity in the DG by Dsp knockdown may also contribute to anxiety-like
591 behavior.

592 Taken together, our findings demonstrate that Dsp in the DG regulates neuronal
593 function and contributes to anxiolytic-like effects. This research uncovers an
594 unexplored function for Dsp in the central nervous system and implies that Dsp in the
595 DG may function as a regulator maintaining proper neuronal activation. Excessive
596 antidepressant treatment can exacerbate neuronal activation, resulting in increased

motor activity (Kobayashi et al., 2010; 2011). Considering the results of these studies and our findings by Dsp knockdown, reduction of Dsp expression by chronic antidepressants in the DG may function as a negative feedback mechanism for excessive neuronal activation rather than merely mediating the effects of antidepressants or anxiolytics.

Limitations of the study

First, although we have proposed a role for Dsp in the nervous system, it is not clear what kind of complexes Dsp forms in neurons. In the future, it will be necessary to investigate what kind of factors Dsp binds to and forms complexes with. Second, we do not know how Dsp regulates neuronal activity and neurogenesis; elucidating the regulation of intracellular signaling by Dsp will improve our understanding of neuronal development and function. Third, it is not clear how Dsp in the DG contributes to emotional behaviors and whether Dsp in the DG contributes to learning and memory. The influence of Dsp in the DG on neural circuits involved in emotion needs to be elucidated. In addition, the role of Dsp in the dorsal DG needs to be investigated for its involvement in learning and memory. Finally, this study shows results in male mice only. It is possible that emotion-related behaviors such as anxiety have different phenotypes depending on sex. Future research should also investigate the role of Dsp in the female nervous system.

Data availability statement

All datasets analyzed in the current study are available from the corresponding author upon reasonable request.

Ethics statement

Animal use and procedures were conducted in accordance with the Tokyo University of Science regulations on animal care and use in research and were approved by the Animal Care and Use Committee of Tokyo University of Science (approval number K20009, K21007, and K22007).

Author contributions: KO, NS, YN, YS, TT, KK, and KS designed the study, conducted the experiments, analyzed the data, and drafted the manuscript. ESN designed the study, analyzed the data, and drafted the manuscript. All the authors have read and approved the final manuscript.

Funding statements: This work was supported in part by MEXT KAKENHI Grants 24K10498 (ESN), 24K09648 (KS), 23H02801(KK and ESN), and 23K18425(KK). Kato Memorial Bioscience Foundation (KS), Brain Science Foundation (KS), Takeda Science Foundation (KS).

Competing interests: The authors declare no competing interests.

Acknowledgements: We would like to thank *Editage* (www.editage.jp) for the English language editing.

References

Allen Institute for Brain Science (2004). Allen Mouse Brain Atlas [https://mouse.brain-map.org/experiment/show/69201504]. Available from mouse.brain-map.org.

Anacker, C., Luna, V.M., Stevens, G.S., Millette, A., Shores, R., Jimenez, J.C., Chen, B., and Hen, R. (2018). Hippocampal neurogenesis confers stress resilience by inhibiting the ventral dentate gyrus. *Nature* 559, 98-102. doi:10.1038/s41586-018-0262-4

Bankhead, P., Loughrey, M.B., Fernandez, J.A., Dombrowski, Y., McArt, D.G., Dunne, P.D., McQuaid, S., Gray, R.T., Murray, L.J., Coleman, H.G., James, J.A., Salto-Tellez, M., and Hamilton, P.W. (2017). QuPath: Open source software for digital pathology image analysis. Sci Rep 7, 16878. doi:10.1038/s41598-017-17204-5

Bendrick, J.L., Eldredge, L.A., Williams, E.I., Haight, N.B., and Dubash, A.D. (2019). Desmoplakin Harnesses Rho GTPase and p38 Mitogen-Activated Protein Kinase Signaling to Coordinate Cellular Migration. *J Invest Dermatol* 139, 1227-1236. doi:10.1016/j.jid.2018.11.032

Broussard, J.A., Getsios, S., and Green, K.J. (2015). Desmosome regulation and signaling in disease. *Cell Tissue Res* 360, 501-512. doi:10.1007/s00441-015-2136-5

Delva, E., Tucker, D.K., and Kowalczyk, A.P. (2009). The desmosome. *Cold Spring Harb Perspect Biol* 1, a002543. doi:10.1101/cshperspect.a002543

Drew, L.J., Fusi, S., and Hen, R. (2013). Adult neurogenesis in the mammalian hippocampus: why the dentate gyrus? *Learn Mem* 20, 710-729. doi:10.1101/lm.026542.112

Dubash, A.D., Kam, C.Y., Aguado, B.A., Patel, D.M., Delmar, M., Shea, L.D., and Green, K.J. (2016). Plakophilin-2 loss promotes TGF-beta1/p38 MAPK-dependent fibrotic gene expression in cardiomyocytes. *J Cell Biol* 212, 425-438. doi:10.1083/jcb.201507018

Fanselow, M.S., and Dong, H.W. (2010). Are the dorsal and ventral hippocampus functionally distinct structures? *Neuron* 65, 7-19. doi:10.1016/j.neuron.2009.11.031

Garcia-Gras, E., Lombardi, R., Giocondo, M.J., Willerson, J.T., Schneider, M.D., Khoury, D.S., and Marian, A.J. (2006). Suppression of canonical Wnt/beta-catenin signaling by nuclear plakoglobin recapitulates phenotype of arrhythmogenic right ventricular cardiomyopathy. *J Clin Invest* 116, 2012-2021. doi:10.1172/JCI27751

Garrod, D., and Chidgey, M. (2008). Desmosome structure, composition and function. *Biochim Biophys Acta* 1778, 572-587. doi:10.1016/j.bbamem.2007.07.014

Imoto, Y., Segi-Nishida, E., Suzuki, H., and Kobayashi, K. (2017). Rapid and stable changes in maturation-related phenotypes of the adult hippocampal neurons by electroconvulsive treatment. *Mol Brain* 10, 8. doi:10.1186/s13041-017-0288-9

Johnson, J.L., Najor, N.A., and Green, K.J. (2014). Desmosomes: regulators of cellular signaling and adhesion in epidermal health and disease. *Cold Spring Harb Perspect Med* 4, a015297. doi:10.1101/cshperspect.a015297

Kempermann, G., Song, H., and Gage, F.H. (2015). Neurogenesis in the Adult Hippocampus. *Cold Spring Harb Perspect Biol* 7, a018812. doi:10.1101/cshperspect.a018812

Kheirbek, M.A., Drew, L.J., Burghardt, N.S., Costantini, D.O., Tannenholz, L., Ahmari, S.E., Zeng, H., Fenton, A.A., and Hen, R. (2013). Differential control of learning and anxiety along the dorsoventral axis of the dentate gyrus. *Neuron* 77, 955-968. doi:10.1016/j.neuron.2012.12.038

Kobayashi, K., Ikeda, Y., Haneda, E., and Suzuki, H. (2008). Chronic fluoxetine bidirectionally modulates potentiating effects of serotonin on the hippocampal mossy fiber synaptic transmission. *J Neurosci* 28, 6272-6280. doi:10.1523/JNEUROSCI.1656-08.2008

Kobayashi, K., Ikeda, Y., Sakai, A., Yamasaki, N., Haneda, E., Miyakawa, T., and Suzuki, H. (2010). Reversal of hippocampal neuronal maturation by serotonergic antidepressants. *Proc Natl Acad Sci U S A* 107, 8434-8439. doi:10.1073/pnas.0912690107

Kobayashi, K., Ikeda, Y., and Suzuki, H. (2011). Behavioral destabilization induced by the selective serotonin reuptake inhibitor fluoxetine. *Mol Brain* 4, 12. doi:10.1186/1756-6606-4-12

Kobayashi, K., Mikahara, Y., Murata, Y., Morita, D., Matsuura, S., Segi-Nishida, E., and Suzuki, H. (2020). Predominant Role of Serotonin at the Hippocampal Mossy Fiber Synapse with Redundant Monoaminergic Modulation. *iScience* 23, 101025. doi:10.1016/j.isci.2020.101025

Kowalczyk, A.P., and Green, K.J. (2013). Structure, function, and regulation of desmosomes. *Prog Mol Biol Transl Sci* 116, 95-118. doi:10.1016/B978-0-12-394311-8.00005-4

Laatsch, R.H., and Cowan, W.M. (1966). Electron microscopic studies of the dentate gyrus of the rat. I. Normal structure with special reference to synaptic organization. *J Comp Neurol* 128, 359-395. doi:10.1002/cne.901280305

Lamothe-Molina, P.J., Franzelin, A., Beck, L., Li, D., Auksutat, L., Fieblinger, T., Laprell, L., Alhbeck, J., Gee, C.E., Kneussel, M., Engel, A.K., Hilgetag, C.C., Morellini, F., and Oertner, T.G. (2022). DeltaFosB accumulation in hippocampal granule cells drives cFos pattern separation during spatial learning. *Nat Commun* 13, 6376. doi:10.1038/s41467-022-33947-w

Levone, B.R., Cryan, J.F., and O'Leary, O.F. (2015). Role of adult hippocampal neurogenesis in stress resilience. *Neurobiol Stress* 1, 147-155. doi:10.1016/j.ynstr.2014.11.003

Lombardi, R., Chen, S.N., Ruggiero, A., Gurha, P., Czernuszewicz, G.Z., Willerson, J.T., and Marian, A.J. (2016). Cardiac Fibro-Adipocyte Progenitors Express Desmosome Proteins and Preferentially Differentiate to Adipocytes Upon Deletion of the Desmoplakin Gene. *Circ Res* 119, 41-54. doi:10.1161/CIRCRESAHA.115.308136

Nestler, E.J., Kelz, M.B., and Chen, J. (1999). DeltaFosB: a molecular mediator of long-term neural and behavioral plasticity. *Brain Res* 835, 10-17. doi:10.1016/s0006-8993(98)01191-3

Newton, S.S., Collier, E.F., Hunsberger, J., Adams, D., Terwilliger, R., Selvanayagam, E., and Duman, R.S. (2003). Gene profile of electroconvulsive seizures: induction of neurotrophic and angiogenic factors. *J Neurosci* 23, 10841-10851. doi:10.1523/JNEUROSCI.23-34-10841.2003

Patel, D.M., Dubash, A.D., Kreitzer, G., and Green, K.J. (2014). Disease mutations in desmoplakin inhibit Cx43 membrane targeting mediated by desmoplakin-EB1 interactions. *J Cell Biol* 206, 779-797. doi:10.1083/jcb.201312110

Paxinos, G.F., K. B. J., 2012. 4th ed. Academic Press., Cambridge, MA.

Rao, S., Kay, Y., and Herring, B.E. (2019). Tiam1 is Critical for Glutamatergic Synapse Structure and Function in the Hippocampus. *J Neurosci* 39, 9306-9315. doi:10.1523/JNEUROSCI.1566-19.2019

Revest, J.M., Dupret, D., Koehl, M., Funk-Reiter, C., Grosjean, N., Piazza, P.V., and Abrous, D.N. (2009). Adult hippocampal neurogenesis is involved in anxiety-related behaviors. *Mol Psychiatry* 14, 959-967. doi:10.1038/mp.2009.15

Sahay, A., and Hen, R. (2007). Adult hippocampal neurogenesis in depression. *Nat Neurosci* 10, 1110-1115. doi:10.1038/nn1969

Santarelli, L., Saxe, M., Gross, C., Surget, A., Battaglia, F., Dulawa, S., Weisstaub, N., Lee, J., Duman, R., Arancio, O., Belzung, C., and Hen, R. (2003). Requirement of hippocampal neurogenesis for the behavioral effects of antidepressants. *Science* 301, 805-809. doi:10.1126/science.1083328

Segi-Nishida, E., Warner-Schmidt, J.L., and Duman, R.S. (2008). Electroconvulsive seizure and VEGF increase the proliferation of neural stem-like cells in rat hippocampus. Proc Natl Acad Sci U S A 105, 11352-11357. doi:10.1073/pnas.0710858105

Segi-Nishida, E., and Suzuki, K. (2022). Regulation of adult-born and mature neurons in stress response and antidepressant action in the dentate gyrus of the hippocampus. *Neurosci Res*. doi:10.1016/j.neures.2022.08.010

Sehara, Y., Hayashi, Y., Ohba, K., Uchibori, R., Urabe, M., Inutsuka, A., Shimazaki, K., Kawai, K., and Mizukami, H. (2022). Higher Transduction Efficiency of AAV5 to Neural Stem Cells and Immature Neurons in Gerbil Dentate Gyrus Compared to AAV2 and rh10. *Hum Gene Ther* 33, 76-85. doi:10.1089/hum.2021.106

Shinohara, R., Taniguchi, M., Ehrlich, A.T., Yokogawa, K., Deguchi, Y., Cherasse, Y., Lazarus, M., Urade, Y., Ogawa, A., Kitaoka, S., Sawa, A., Narumiya, S., and Furuyashiki, T. (2018). Dopamine D1 receptor subtype mediates acute stress-induced dendritic growth in excitatory neurons of the medial prefrontal cortex and contributes to suppression of stress susceptibility in mice. *Mol Psychiatry* 23, 1717-1730. doi:10.1038/mp.2017.177

Simon, R., Brylka, H., Schwegler, H., Venkataramanappa, S., Andratschke, J., Wiegreffe, C., Liu, P., Fuchs, E., Jenkins, N.A., Copeland, N.G., Birchmeier, C., and Britsch, S. (2012). A dual function of Bcl11b/Ctip2 in hippocampal neurogenesis. *EMBO J* 31, 2922-2936. doi:10.1038/emboj.2012.142

Ueno, M., Sugimoto, M., Ohtsubo, K., Sakai, N., Endo, A., Shikano, K., Imoto, Y., and Segi-Nishida, E. (2019). The effect of electroconvulsive seizure on survival, neuronal differentiation, and expression of the maturation marker in the adult mouse hippocampus. *J Neurochem* 149, 488-498. doi:10.1111/jnc.14691

Wang, J.W., David, D.J., Monckton, J.E., Battaglia, F., and Hen, R. (2008). Chronic fluoxetine stimulates maturation and synaptic plasticity of adult-born hippocampal granule cells. *J Neurosci* 28, 1374-1384. doi:10.1523/JNEUROSCI.3632-07.2008

Warner-Schmidt, J.L., and Duman, R.S. (2007). VEGF is an essential mediator of the neurogenic and behavioral actions of antidepressants. *Proc Natl Acad Sci U S A* 104, 4647-4652. doi:10.1073/pnas.0610282104

Yamasaki, N., Maekawa, M., Kobayashi, K., Kajii, Y., Maeda, J., Soma, M., Takao, K., Tanda, K., Ohira, K., Toyama, K., Kanzaki, K., Fukunaga, K., Sudo, Y., Ichinose, H., Ikeda, M., Iwata, N., Ozaki, N., Suzuki, H., Higuchi, M., Suhara, T., Yuasa, S., and Miyakawa, T. (2008). Alpha-CaMKII deficiency causes immature dentate gyrus, a novel candidate endophenotype of psychiatric disorders. *Mol Brain* 1, 6. doi:10.1186/1756-6606-1-6

You, J.C., Muralidharan, K., Park, J.W., Petrof, I., Pyfer, M.S., Corbett, B.F., LaFrancois, J.J., Zheng, Y., Zhang, X., Mohila, C.A., Yoshor, D., Rissman, R.A., Nestler, E.J., Scharfman, H.E., and Chin, J. (2017). Epigenetic suppression of hippocampal calbindin-D28k by DeltaFosB drives seizure-related cognitive deficits. *Nat Med* 23, 1377-1383. doi:10.1038/nm.4413

Zhao, C., Deng, W., and Gage, F.H. (2008). Mechanisms and functional implications of adult neurogenesis. *Cell* 132, 645-660. doi:10.1016/j.cell.2008.01.033

Figure legends

Figure 1. Expression of Dsp in the dentate gyrus (DG) of the hippocampus

(A) Expression of Dsp mRNA in adult mouse brain from Allen Mouse Brain Atlas. (B) Low magnification images of immunoreactivity for Dsp (magenta) in the DG and CA1. DAPI (cyan) is utilized for nuclear staining. GCL; granule cell layer, ML; molecular layer. Scale bar: 200 μm. (C) Representative images of immunoreactivity for Dsp (green), NeuN (upper, magenta), and NeuroD1 (lower, magenta) in the DG. DAPI was used for nuclear staining (blue). Enlarged images of the dotted square are shown below. Arrows represent Dsp-negative and NeuroD1-positive cells (arrows). Scale bars: 50 μm. (D) Relative gene expression of *Dsp* at 24 h after 11 times of electroconvulsive seizure (ECS) stimulation (left, P=0.0324) or 4-weeks treatment of selective serotonin reuptake inhibitor (SSRI) fluoxetine (right, P=0.0057). Data are expressed using dot plots and means ± standard error of mean. The n number is given in graph. *, $P<0.05$; **, $P<0.01$. Detailed statistical data are shown in Table 2. (E) Representative images of immunoreactivity for Dsp (green) in the DG after 11 or 20 times of ECS stimulation. Scale bars: 20 μm.

Figure 2. Knockdown of Dsp in the DG by adeno-associated virus (AAV) carrying Dsp artificial miRNA and expression changes in the DG

(A) Structure of AAVrh10 carrying EGFP and artificial microRNA sequence for Dsp (DSP miRNA) and time course of experimental procedure. Representative EGFP image 7–8 weeks after control miRNA AAV injection into the DG (left). EGFP and immunoreactivity for an immature neuronal marker doublecortin (magenta) in the DG (right). (B) Gene expression of *Dsp* 7–8 weeks after AAV infection (P=0.0482). (C) Representative images of immunoreactivity for Dsp (red) and DAPI (blue) in the DG

821 after AAV infection. (D) Effect of Dsp knockdown in the DG on the expression of FosB
822 protein. Representative images of immunoreactivity for FosB in the DG (left).
823 Quantification of FosB-positive cell numbers (right) in the granule cell layer
824 (P=0.0002). (E) Effect of Dsp knockdown in the DG on the expression of DG specific
825 maturation markers in the DG. Expression of *Calb1* (P=0.0232), *Tdo2* (P=0.0195), *Ntf3*
826 (P=0.00039), and *Il1r1* (P=0.5926). Data are expressed using dot plots and means ±
827 standard error of mean. The n number is given in graph. *, $P<0.05$; **, $P<0.01$; ***,
828 $P<0.001$; n.s., not significant. Detailed statistical data are shown in Table 2. Scale bars:
829 1 mm for the low magnification image in Fig. 2A (left); 100 μm for other images.
830
831 **Figure 3. Electrophysiological changes in the DG by Dsp knockdown**
832 (A) Diagram showing the electrode arrangement for recording field excitatory post
833 synaptic potentials (EPSPs) at the medial perforant path (MPP)–granule cell synapse.
834 (B) Sample recordings show MPP synaptic potentials evoked at the stimulus intensities
835 of 2, 3, 4 and 5 V in control DG and knockdown DG. (C) The relationship between
836 fiber volley and EPSP at MPP–DG synapse. (D) Diagram showing for recording field
837 EPSPs at the mossy fiber (MF)–CA3 synapse. (E) Ratios for MF field EPSPs to fiber
838 volley (FV) at the baseline stimulus intensity (P=0.3406). (F and G) Effect of Dsp
839 knockdown on synaptic facilitation induced by repetitive stimulation at the MF synapse
840 (G, P=0.9387). (H) Effect of Dsp knockdown on potentiation of MF synaptic
841 transmission induced by serotonin (5 μM, 5 min) applied in the bath. Sample recordings
842 show averages of nine consecutive field EPSPs before and at the end of serotonin
843 application in control DG and knockdown DG. (I) Effect of Dsp knockdown on
844 serotonin-induced synaptic potentiation (P=0.0032). (J) Representative images of Golgi
845 staining in the DG (left) and dendrites (right) in inner molecular layer. (K) Quantitative

analysis of the number of spines in the dendrites. Ten dendrites per animal and six mice per group were analyzed. Data are expressed using dot plots and means ± standard error of mean. The n number of data is given in graph and represents the number of slices (E, G, I) and dendrites (K). **, *P*<0.01. Detailed statistical data are shown in Table 2.

Figure 4. Adult neurogenic changes in the DG by Dsp knockdown

(A) Effect of Dsp knockdown on proliferation in the DG. Left: Time course of the experimental procedure. Middle: Representative images of immunoreactivity for BrdU (red). The arrows represent BrdU-positive cells in the SGZ. Scale bars: 20 μm. Right: Quantification of BrdU-positive cell numbers in the SGZ (P=0.6175). (B) Effect of Dsp knockdown on the number of neural stem cells or progenitors in the DG. Left: Representative images of immunoreactivity for SOX2 in the DG. Scale bars: 100 μm. Right: Quantification of SOX2-positive cell numbers in the SGZ (P=0.2652).

(C) Effect of Dsp knockdown on neuronal differentiation in the DG. Left: Representative images of immunoreactivity for NeuroD1 in the DG. Scale bars: 100 μm. Right: Quantification of NeuroD1-positive cell numbers in the SGZ (P=0.0015). (D) Effect of Dsp knockdown on cell number of doublecortin (DCX)-positive immature neurons in the DG. Left: Representative images of immunoreactivity for DCX in the DG. Scale bars: 40 μm. Middle: Quantification of DCX-positive cell numbers in the SGZ (P=0.0149). Right: Quantification of DCX-positive cells with long dendrites in the SGZ (P=0.0374). (E) Effect of Dsp knockdown on survival of 2-weeks of cell age in the DG. Left: Time course of the experimental procedure. Middle: Quantification of BrdU-positive cells of 2-weeks (2 wks) of cell age in the DG (P=0.1715). Right: The ratio of NeuN(+) cells among the BrdU (+) cells in the DG (P=0.3394).

Data are expressed using dot plots and means ± standard error of mean. The n number is given in graph. *, $P<0.05$; **, $P<0.01$. n.s. not significant. Detailed statistical data are shown in Table 2.

Figure 5. Behavioral changes in the DG by Dsp knockdown

(A) Time course of the experimental procedure. (B) Exploratory behaviors of open field test (OFT). Total distance (left, P=0.0071) in the open field. Time spent (middle, P=0.1071) and entry times (right, P=0.0450) in the center of the open field. (C) Immobility time in the forced swim test (FST, P=0.5065). (D) Total distance of locomotor activity (LMA) in the home cage (P=0.3558). (E) Social interaction behavior in the 3-chamber social interaction test (SIT). A stranger mouse within a wire cup placed in one chamber (social) and an empty wire cup placed in another chamber (Non-Social). (F) Time spent on the open arms (left, P=0.0495) and total distance (right, P=0.0262) in the elevate plus maze (EPM) test. Data are expressed using dot plots and means ± standard error of mean. The n number is given in graph. *, $P<0.05$; **, $P<0.01$; n.s. not significant. Detailed statistical data are shown in Table 2.

Table 1. List of primers used for qPCR analysis.

Gene	Forward (5' to 3')	Reverse (5' to 3')
Dsp	GCTGAAGAACACTCTAGCCCA	ACTGCTGTTTCCTCTGAGACA
Calb1	TCTGGCTTCATTTCGACGCTG	ACAAAGGATTTCATTTCCGGTGA
Tdo2	ATGAGTGGGTGCCCGTTTG	GGCTCTGTTTACACCAGTTTGAG
Ntf3	AGTTTGCCGGAAGACTCTCTC	GGGTGCTCTGGTAATTTTCCTTA
Il1r1	GTGCTACTGGGGCTCATTTGT	GGAGTAAGAGGACACTTGCGAAT
Hdac2	GGAGGAGGCTACACAATCCG	TCTGGAGTGTTCTGGTTTGTCA
Tiam1	AGACTGAACGCACCTATGTGA	ACTCGACTTGAAACTCCACCAT
18S	GAGGCCCTGTAATTGGAATGAG	GCAGCAACTTTAATATACGCTATTGG
Gapdh	AGGTCGGTGTGAACGGATTTG	TGTAGACCATGTAGTTGAGGTCA

Table 2. Statistical analysis

		F value	Statistical Test	T value	P value
Figure 1D; *Dsp*	CNT, n=3 ECS, n=4	F(2,3)=22.92, P=0.0304	Unpaired t test with Welch's correction	t(5.504)=2.131	P=0.0324
Figure 1D; *Dsp*	CNT, n=7 SSRI, n=7	F(6,6)=7.606, P=0.0262	Unpaired t test with Welch's correction	t(7.551)=3.818	P=0.0057
Figure 2B; *Dsp*	CNT, n=9 KD, n=9	F(8,8)=6.584, P=0.0152	Unpaired t test with Welch's correction	t(10.38)=2.239	P=0.0482
Figure 2D; FosB(+)	CNT, n=4 KD, n=3	F(3,2)=1.636, P=0.8023	Unpaired t test	t(5)=10.17	P=0.0002
Figure 2E; *Calb*	CNT, n=8 KD, n=9	F(7,6)=3.495, P=0.1485	Unpaired t test	t(13)=2.572	P=0.0232
Figure 2E; *Tdo2*	CNT, n=7 KD, n=8	F(7,6)=4.257, P=0.0974	Unpaired t test	t(13)=2.662	P=0.0195
Figure 2E; *Ntf3*	CNT, n=9 KD, n=9	F(8,8)=1.275, P=0.7396	Unpaired t test	t(16)=3.373	P=0.00039
Figure 2E; *Il1r1*	CNT, n=9 KD, n=9	F(8,8)=1.006, P=0.9933	Unpaired t test	t(16)=0.5359	P=0.5926
Figure 3B; EPSP/FV	CNTDG,n=9 KD DG, n=9	F(8,8)=1.362, P=0.6994	Unpaired t test	t(16)=0.9823	P=0.3406
Figure 3D; 1Hz facilitation	CNTDG,n=7 KDDG n=7	F(6,6)=2.402, P=0.3104	Unpaired t test	t(12)=0.07857	P=0.9387
Figure 3 ; Spines	CNT, n=60 KD n=60 (dendrites)	F(59,59)=1.206, P=0.4739	Unpaired t test	t(118)=2.372	P=0.0193
Figure 3F; serotonin	CNTDG,n=5 KDDG, n=5	F(4,4)=2.407, P=0.4158	Unpaired t test	t(8)=4.158	P=0.0032
Figure 4A; proliferation	CNT, n=7 KD, n=5	F(6,4)=3.905, P=0.2083	Unpaired t test	t(10)=0.5153	P=0.6175

Figure 4B; SOX2(+)	CNT, n=6 KD, n=6	F(5,5)=1.942, P=0.4838	Unpaired t test	t(10)=1.180	P=0.2652
Figure 4C; NeuroD1(+)	CNT, n=6 KD, n=6	F(5,5)=4.677, P=0.1157	Unpaired t test	t(10)=4.338	P=0.0015
Figure 4D; DCX(+)	CNT, n=5 KD, n=6	F(4,5)=6.073, P=0.0740	Unpaired t test	t(9)=3.001	P=0.0149
Figure 4D; long-DCX(+)	CNT, n=5 KD, n=6	F(4,5)=7.397, P=0.0499	Unpaired t test with Welch's correction	t(4.902)=2.833	P=0.0374
Figure 4E; survival	CNT, n=5 KD, n=6	F(4,5)=1.843, P=0.5170	Unpaired t test	t(9)=1.486	P=0.1715
Figure 4E; BrdUNeuN	CNT, n=4 KD, n=5	F(3,4)=1.424, P=0.7193	Unpaired t test	t(7)=1.025	P=0.3394
Figure 5B; OFT	CNT, n=8 KD, n=11	Grubbs outlier (center)	CNT, n=1 KD, n=1	G=2.144 G=2.804	
distance	CNT, n=7 KD, n=10	F(6,9)=1.800, P=0.4109	Unpaired t test	t(15)=3.112	P=0.0071
center	CNT, n=7 KD, n=10	F(6,9)=1.202, P=0.7715	Unpaired t test	t(15)=1.714	P=0.1071
entry	CNT, n=7 KD, n=10	F(6,9)=3.532, P=0.13	Unpaired t test	t(15)=2.187	P=0.0450
Figure 5C; FST	CNT, n=7 KD, n=8	F(6,7)=2.652, P=0.2279	Unpaired t test	t(13)=0.6832	P=0.5065
Figure 5D; LMA	CNT, n=18 KD, n=17	F(17,16)=1.416, P=0.4915	Unpaired t test	t(33)=0.9365	P=0.3558
Figure 5E; SIT time in zone	CNT, n=17 KD, n=15	Two-way ANOVA	interaction	F(1,60)=0.5081	P=0.4787
			knockdown	F(1,60)=0.2990	P=0.5865
			social state	F(1,60)=41.97	P<0.0001
Figure 5F; EPM, Open	CNT, n=18 KD, n=17	F(17,16)=2.849, P=0.0419	Unpaired t test with Welch's correction	t(27.89)=2.054	P=0.0495
Figure 5F; EPM, Distance	CNT, n=18 KD, n=17	F(17,16)=1.683 P=0.3043	Unpaired t test	t(33)=2.329	P=0.0262

A

Dsp mRNA
in situ hybridization

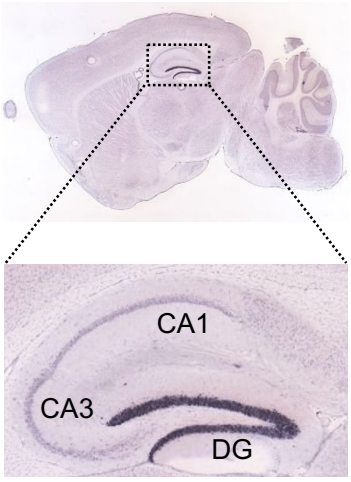

B

Dsp Immunohistochemistry

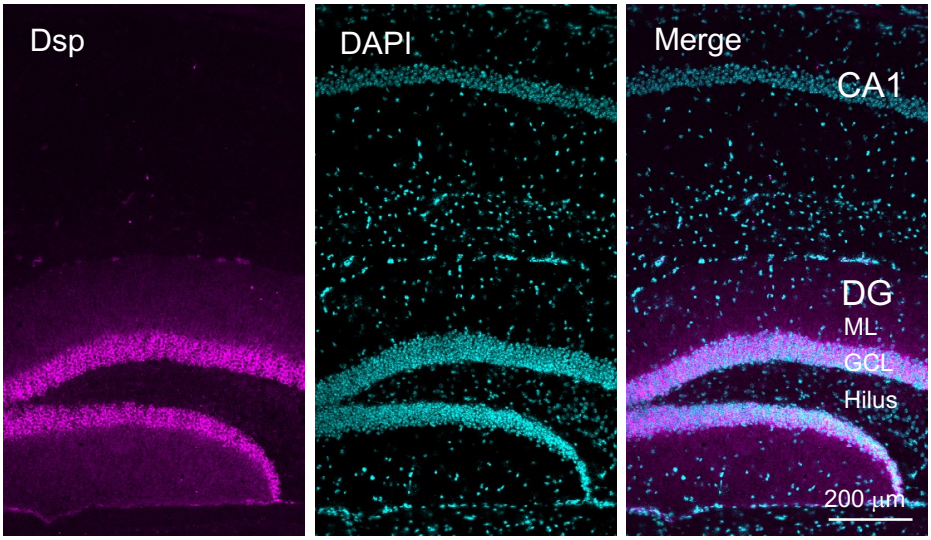

C

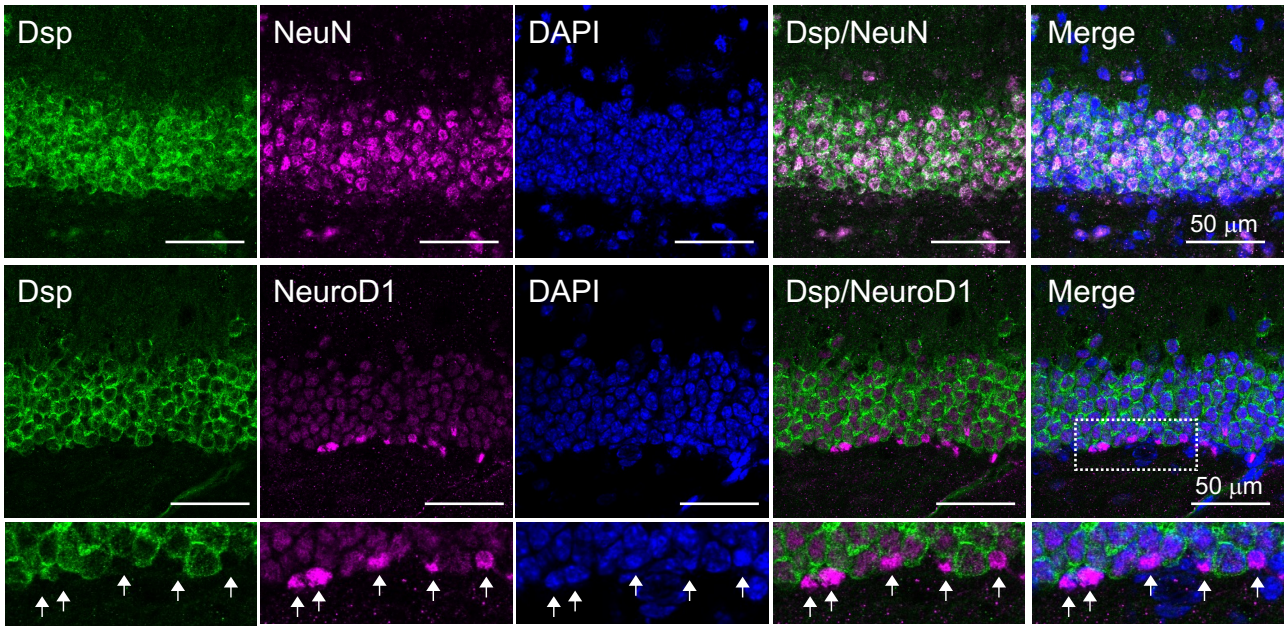

D

Dsp mRNA expression

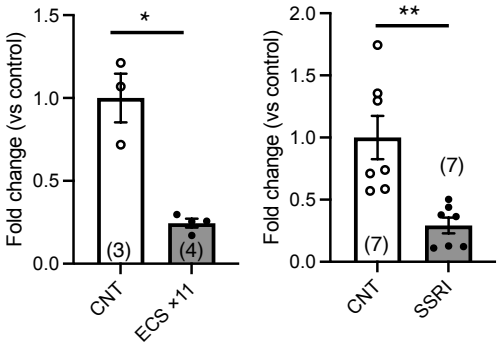

E

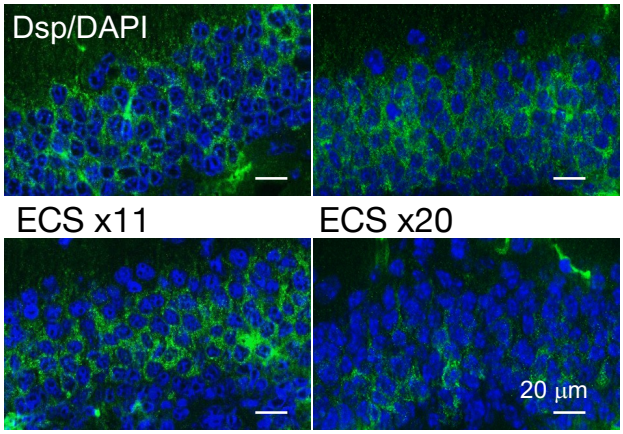

Figure 1

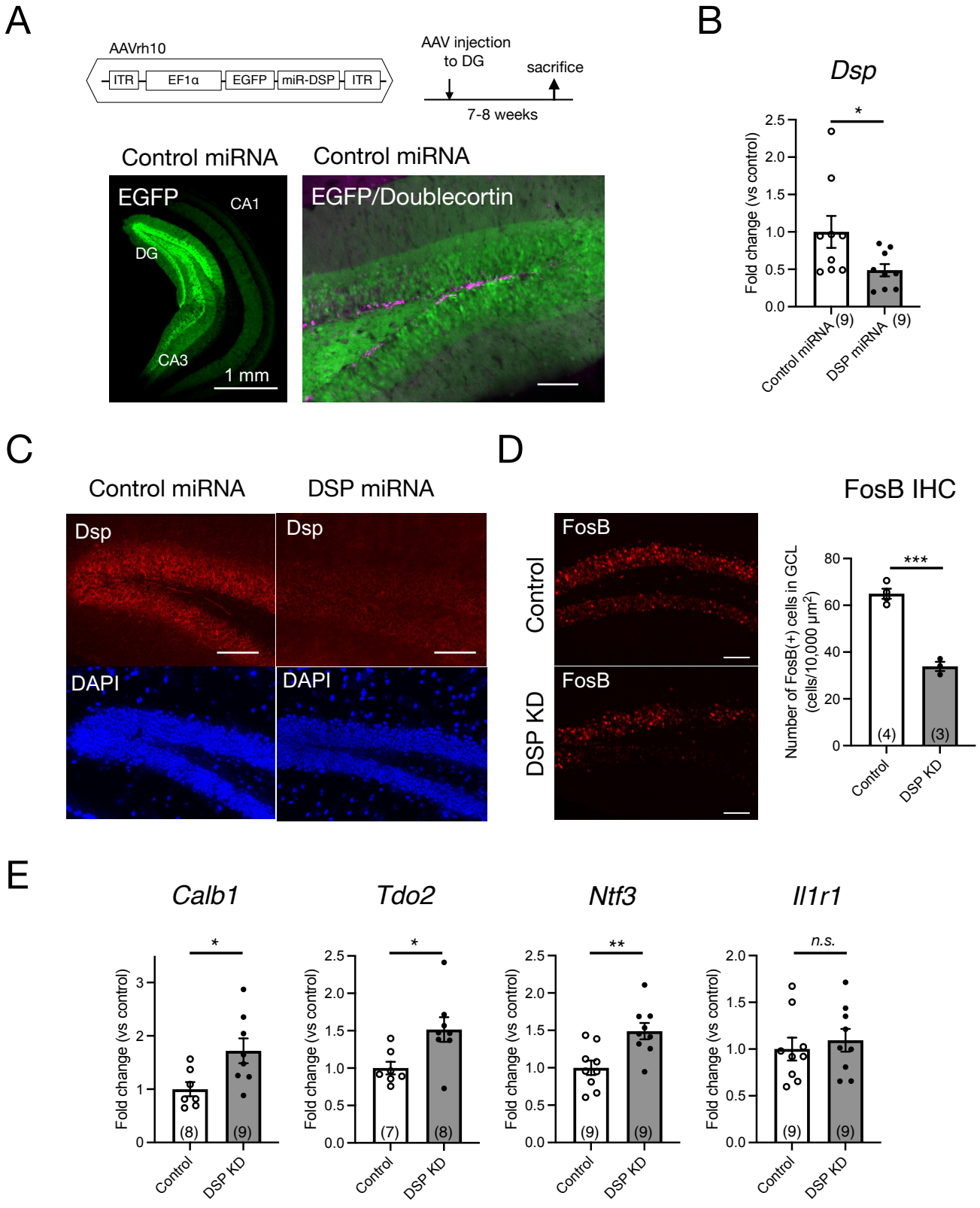
A
AAVrh10
ITR
EF1α
EGFP
miR-DSP
ITR
AAV injection to DG
sacrifice
7-8 weeks
Control miRNA
Control miRNA
EGFP
CA1
DG
CA3
1 mm
EGFP/Doublecortin
B
Dsp
Fold change (vs control)
Control miRNA
DSP miRNA
(9)
(9)
C
Control miRNA
DSP miRNA
Dsp
Dsp
DAPI
DAPI
D
FosB IHC
Control
DSP KD
FosB
FosB
Number of FosB(+) cells in GCL (cells/10,000 μm²)
Control
DSP KD
(4)
(3)
E
Calb1
Tdo2
Ntf3
Il1r1
Fold change (vs control)
n.s.
Control
DSP KD

Figure 2

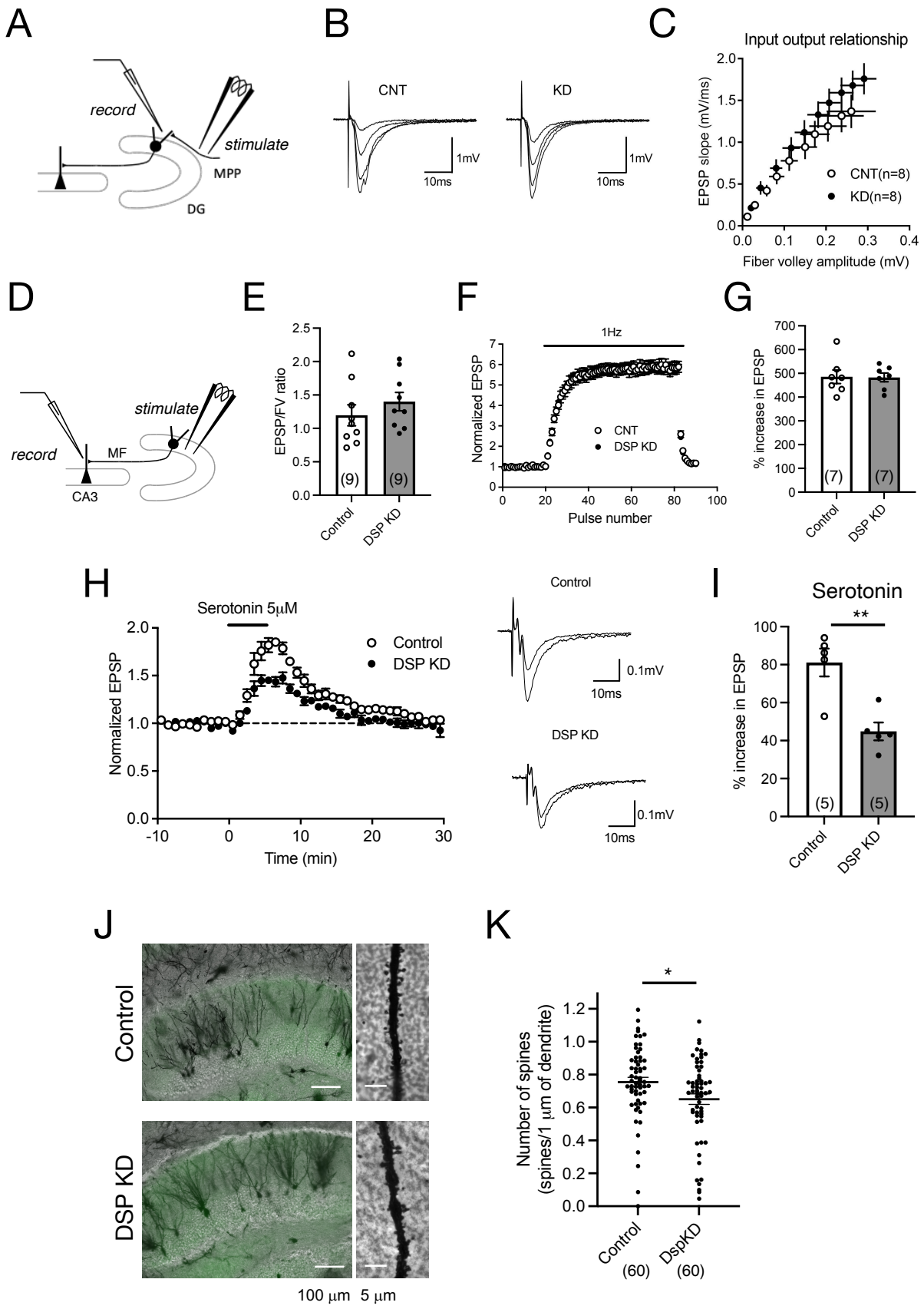
A
record
stimulate
MPP
DG
B
CNT
KD
1mV
10ms
C
Input output relationship
EPSP slope (mV/ms)
Fiber volley amplitude (mV)
CNT(n=8)
KD(n=8)
D
stimulate
record
MF
CA3
E
EPSP/FV ratio
(9)
(9)
Control
DSP KD
F
1Hz
Normalized EPSP
CNT
DSP KD
Pulse number
G
% increase in EPSP
(7)
(7)
Control
DSP KD
H
Serotonin 5μM
Normalized EPSP
Control
DSP KD
Time (min)
Control
DSP KD
0.1mV
10ms
I
Serotonin
**
% increase in EPSP
(5)
(5)
Control
DSP KD
J
Control
DSP KD
100 μm
5 μm
K
*
Number of spines
(spines/1 μm of dendrite)
Control
DspKD
(60)
(60)

Figure 3

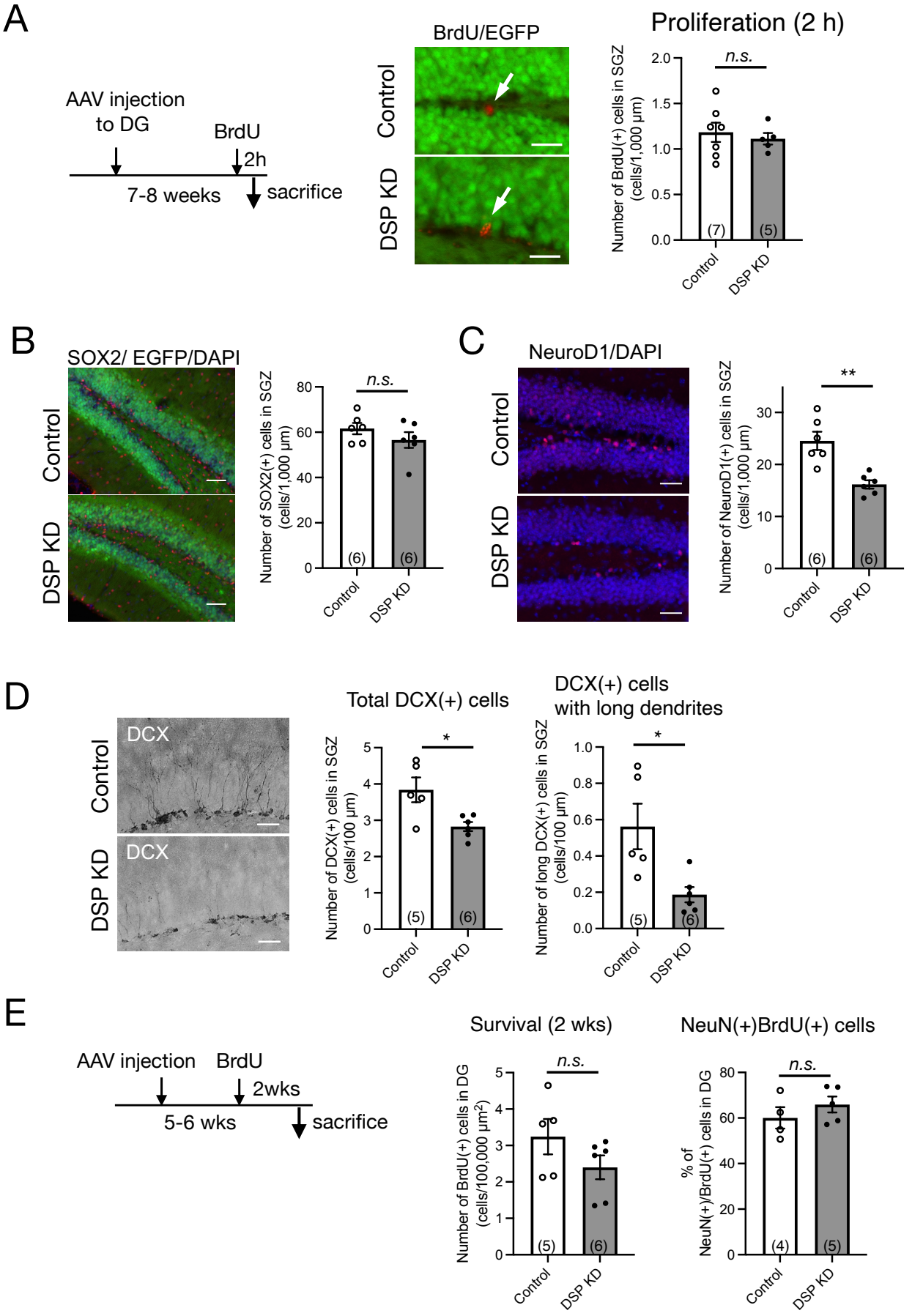
A
AAV injection
to DG
BrdU
2h
7-8 weeks
sacrifice
BrdU/EGFP
Control
DSP KD
Proliferation (2 h)
n.s.
Number of BrdU(+) cells in SGZ
(cells/1,000 μm)
2.0
1.5
1.0
0.5
0.0
(7)
(5)
Control
DSP KD
B
SOX2/ EGFP/DAPI
Control
DSP KD
n.s.
Number of SOX2(+) cells in SGZ
(cells/1,000 μm)
80
60
40
20
0
(6)
(6)
Control
DSP KD
C
NeuroD1/DAPI
Control
DSP KD
**
Number of NeuroD1(+) cells in SGZ
(cells/1,000 μm)
30
20
10
0
(6)
(6)
Control
DSP KD
D
DCX
Control
DCX
DSP KD
Total DCX(+) cells
*
Number of DCX(+) cells in SGZ
(cells/100 μm)
5
4
3
2
1
0
(5)
(6)
Control
DSP KD
DCX(+) cells
with long dendrites
*
Number of long DCX(+) cells in SGZ
(cells/100 μm)
1.0
0.8
0.6
0.4
0.2
0.0
(5)
(6)
Control
DSP KD
E
AAV injection
BrdU
2wks
5-6 wks
sacrifice
Survival (2 wks)
n.s.
Number of BrdU(+) cells in DG
(cells/100,000 μm²)
5
4
3
2
1
0
(5)
(6)
Control
DSP KD
NeuN(+)BrdU(+) cells
n.s.
% of
NeuN(+)/BrdU(+) cells in DG
80
60
40
20
0
(4)
(5)
Control
DSP KD

Figure 4

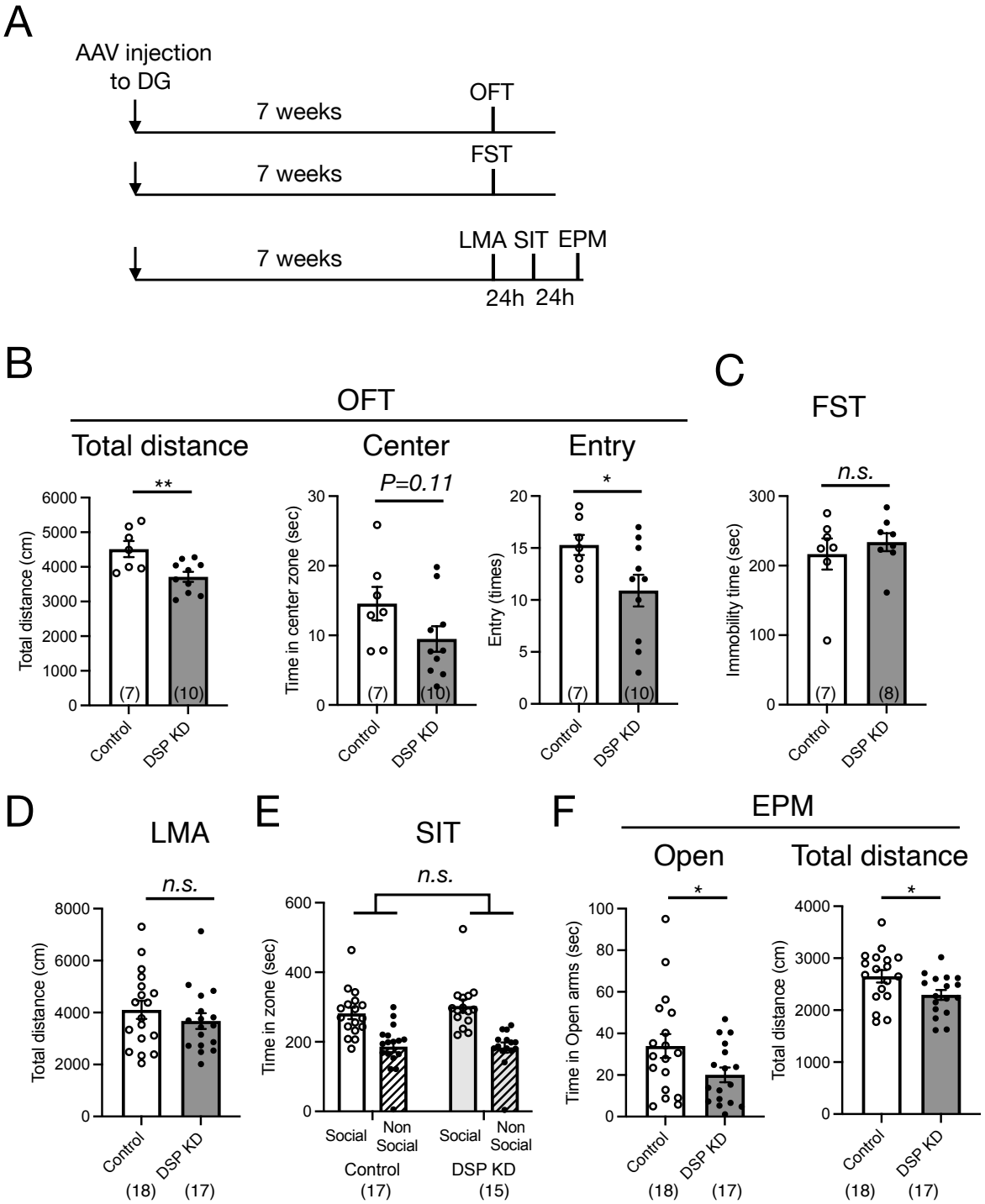
A
AAV injection
to DG
7 weeks
OFT
7 weeks
FST
7 weeks
LMA SIT EPM
24h 24h
B
OFT
Total distance
Center
Entry
**
P=0.11
*
Total distance (cm)
Time in center zone (sec)
Entry (times)
Control
DSP KD
(7)
(10)
C
FST
n.s.
Immobility time (sec)
(8)
D
LMA
n.s.
(18)
(17)
E
SIT
n.s.
Time in zone (sec)
Social
Non Social
Control
DSP KD
(17)
(15)
F
EPM
Open
Total distance
Time in Open arms (sec)

Figure 5